

ABSOLUTE RADIOMETRIC CALIBRATION OF THE EUNIS-06 170–205 Å CHANNEL AND CALIBRATION UPDATE FOR CDS/NIS

TONGJIANG WANG^{1,2}, JEFFREY W. BROSIUS^{1,2}, ROGER J. THOMAS², DOUGLAS M. RABIN², AND JOSEPH M. DAVILA²
submitted to ApJ Supplement

ABSTRACT

The Extreme-Ultraviolet Normal-Incidence Spectrograph sounding-rocket payload was flown on 2006 April 12 (EUNIS-06), carrying two independent imaging spectrographs covering wave bands of 300–370 Å in first order and 170–205 Å in second order, respectively. The absolute radiometric response of the EUNIS-06 long-wavelength (LW) channel was directly measured in the same facility used to calibrate CDS prior to the *SOHO* launch. Because the absolute calibration of the short-wavelength (SW) channel could not be obtained from the same lab configuration, we here present a technique to derive it using a combination of solar LW spectra and density- and temperature-insensitive line intensity ratios. The first step in this procedure is to use the coordinated, cospatial EUNIS and *SOHO*/CDS spectra to carry out an intensity calibration update for the CDS NIS-1 waveband, which shows that its efficiency has decreased by a factor about 1.7 compared to that of the previously implemented calibration. Then, theoretical insensitive line ratios obtained from CHIANTI allow us to determine absolute intensities of emission lines within the EUNIS SW bandpass from those of cospatial CDS/NIS-1 spectra after the EUNIS LW calibration correction. A total of 12 ratios derived from intensities of 5 CDS and 12 SW emission lines from Fe X–Fe XIII yield an instrumental response curve for the EUNIS-06 SW channel that matches well to a relative calibration which relied on combining measurements of individual optical components. Taking into account all potential sources of error, we estimate that the EUNIS-06 SW absolute calibration is accurate to $\pm 20\%$.

Subject headings: instrumentation: spectrographs — Sun: activity — Sun: corona — Sun: UV radiation

1. INTRODUCTION

The extreme-ultraviolet (EUV) waveband (150–1200 Å) contains emission lines formed at temperatures ranging from several times 10^4 K to several times 10^7 K and is therefore well suited for studies of the multithermal structures in the solar atmosphere. The Solar EUV Research Telescope and Spectrograph (SERTS) sounding rocket payload (Neupert et al. 1992) was developed at NASA’s GSFC to study the Sun’s corona and upper transition region with imaged EUV spectra. It was flown ten times, and produced excellent quality, high resolution spectra (e.g. Thomas & Neupert 1994; Brosius et al. 1996, 1997, 1998a,b, 1999, 2000; Andretta et al. 2000). Several SERTS flights have provided updated radiometric calibrations for the Coronal Diagnostic Spectrometer (CDS; Harrison et al. 1995) on the *Solar and Heliospheric Observatory (SOHO)* mission (e.g. Thomas 2002).

EUNIS (EUV Normal-Incidence Spectrograph) is a next-generation EUV imaging spectrograph that is 100 times more sensitive than SERTS, with $\sim 5''$ spatial resolution and ~ 2 s time cadence (Thomas & Davila 2001). This powerful instrument can pave the way for entirely new studies of the corona using high cadence spectra at a single location, rapid rastering over large 2D areas of the solar surface, or deep exposures on intrinsically faint coronal features. EUNIS has now been

successfully flown twice, in April 2006 and November 2007 (Rabin, Thomas & Brosius 2008). Scientific results have already been reported using the EUNIS-06 data. For example, Brosius, Rabin, & Thomas (2007) found both upflows and downflows in a coronal bright point observed in emission lines formed at $T=0.05\text{--}2.5$ MK, providing evidence for magnetic reconnection in bright points. Brosius, Rabin, & Thomas (2008) further derived coronal electron densities, the differential emission measure, and elemental abundances of this bright point from line intensities. Brosius et al. (2008) studied a cool transient event seen only in He II with high-cadence spectra, revealing relative upflows up to 20 km s^{-1} which are consistent with gentle chromospheric evaporation. Jess et al. (2008) found short-period (26 ± 4 s) velocity oscillations in the He II 303.8 Å line and other transition region (TR) lines formed at temperatures up to 4×10^5 K and suggested an interpretation in terms of fast sausage modes in a flux tube.

For EUNIS-06, a complete end-to-end radiometric calibration of its long wavelength (LW) channel was carried out at the Rutherford Appleton Laboratory (RAL) in England using a stable EUV transfer light source provided by the German Physikalisch-Technische Bundesanstalt (PTB). Unfortunately, it was not possible to obtain a similar measurement of the EUNIS short-wavelength (SW) channel due to the weakness of available lines in that waveband. Therefore, we have developed a technique for deriving the absolute radiometric calibration of its SW channel by combining measured LW solar spectra with density- and temperature-insensitive line intensity ratios. The procedure of using insensi-

¹ Department of Physics, Catholic University of America, 620 Michigan Avenue NE, Washington, DC 20064, USA; wangtj@helio.gsfc.nasa.gov

² NASA Goddard Space Flight Center, Code 671, Greenbelt, MD 20771, USA

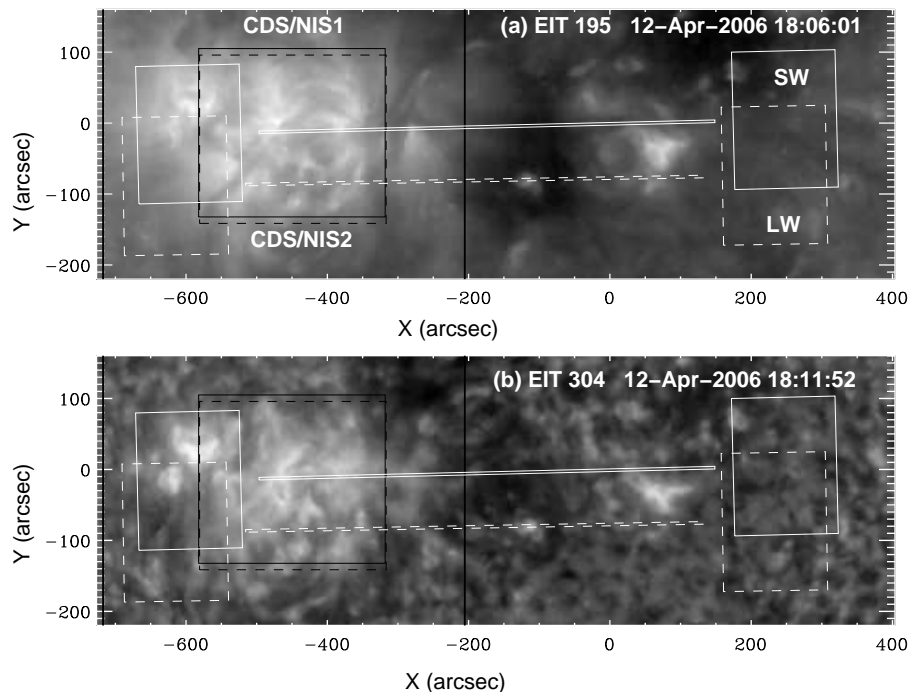


FIG. 1.— Coalignments of the pointing for EUNIS-06 LW and SW channels with SOHO/CDS NIS-1 and NIS-2, SOHO/EIT, and TRACE. The overlaid images are (a) EIT 195 Å and (b) EIT 304 Å. The slit and two lobes positions for EUNIS SW and LW channels are marked with white solid and dashed lines, respectively. The FOVs for CDS/NIS-1 and NIS-2 are marked with black solid and dashed lines, respectively. Two vertical, black and thick solid lines mark the left and right boundaries of the FOV for TRACE.

tive line intensity ratios to derive relative radiometric calibration was first suggested by Neupert & Kastner (1983) and has been successfully applied in calibrations of SERTS and other instruments.

2. OBSERVATIONS AND DATA REDUCTION

EUNIS-06 was launched from White Sands Missile Range, New Mexico, at 18:10 UT on 2006 April 12. It achieved a maximum altitude of 313 km and obtained solar spectra and images between 1812 and 1818 UT. EUNIS observed NOAA AR 10871 (S07°, E28°) and AR 10870 (S08°, W02°), the quiet region between them and a southern-hemisphere coronal bright point within the quiet area (Brosius, Rabin, & Thomas 2007; Brosius et al. 2008). Coordinated observations were obtained with the EUV Imaging Telescope (EIT; Delaboudinière et al. 1995) and the CDS aboard *SOHO*, as well as with the *Transition Region and Coronal Explorer* (TRACE; Handy et al. 1999). We coaligned the data from different instruments with a cross-correlation method, taking the EIT images as a reference.

2.1. EUNIS

The optical design of EUNIS is directly based on that of SERTS, but features two independent, imaging spectrographs, one covering EUV lines between 300 and 370 Å seen in first order (LW channel), and a second covering lines between 170 and 205 Å seen in second order (SW channel). For both channels, the optical design of telescope, entrance slit, toroidal grating, and detector are identical, with the only difference being the multi-layer coatings applied to the reflecting surfaces. Each channel includes a microchannel-plate (MCP) intensifier section and a set of three 1K×1K active pixel sensors

(APS), which are coupled to the MCP by fine-pore fiberoptic blocks. Areas of the solar image selected by the two entrance apertures include a narrow 2''×660'' slit along which spatially resolved spectra are obtained, and wider “lobes” at the ends from which spectroheliograms are obtained. For this flight, the lobe-slit fields of view were oriented East-West near the center of the solar disk. EUNIS has a first-order spectral dispersion of 25 mÅ pixel⁻¹ and a designed spatial scale of 0''.927 pixel⁻¹. A more detailed description of EUNIS design was given by Thomas & Davila (2001). For the first flight of EUNIS, its optics limited the actual spatial resolution to about 5'' and the measured spectral resolution was ~200 and ~100 mÅ FWHM in the LW and SW channels.

In this first flight we obtained 80 solar exposures in “stare” (fixed pointing) mode at the start of the flight with ~2 s cadence for all but the first five; further observations were made in scanning (spectroheliogram) mode. All of the raw data were processed with several routine adjustments, including dark image subtraction, flat-fielding and non-linearity correction. The quality of our EUNIS data is sufficient to reveal non-linearities in the APS response that reach about 15% as they approach saturation. This effect is identical for all APS units, and has been characterized by ratios of different exposure times to a constant EUV source in the laboratory. Appropriate corrections for the effect are applied to raw data to convert the recorded Data Numbers (DN) into Relative Exposure Units (REU), which are then used in all subsequent analyses. We used 34 exposures of the stare sequence to create an averaged lobe image for coalignments and an averaged spectral image for calibration.

2.2. SOHO/CDS

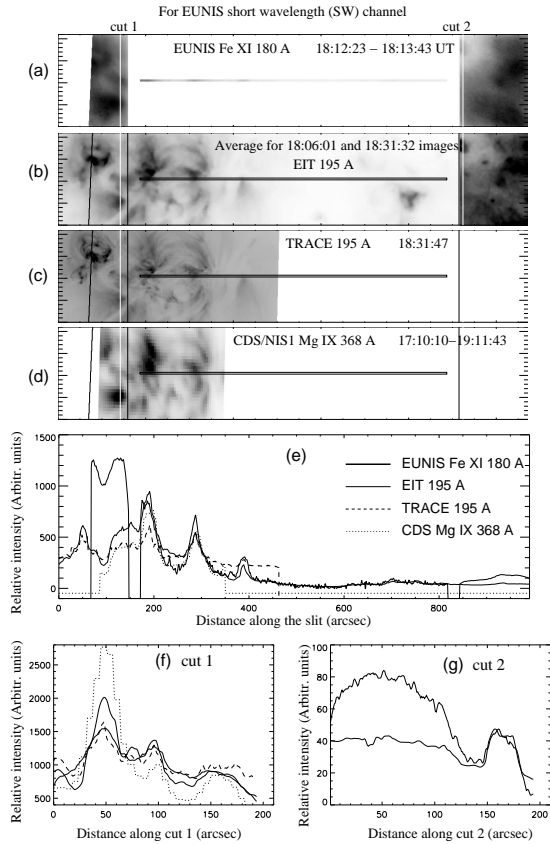


FIG. 2.— Comparisons of images and intensity profiles from observations of different instruments. (a) Image of Fe XI 180 Å line intensity from the EUNIS-06 SW channel. The EUNIS SW slit is the nearly-horizontal line toward the center of panels (a)-(d). (b) The EIT 195 Å image, in which the contrast in the right lobe is enhanced in order to be seen clearly. (c) The TRACE 195 Å image. (d) The Mg IX 368 Å line intensity image from CDS/NIS-1. (e) Comparisons of intensity profiles along the EUNIS slit (including its extending in two lobes). (f) and (g) Comparisons of intensity profiles along cut1 and cut2 (white vertical lines) marked in (a), respectively.

The CDS includes a Normal Incidence Spectrometer (NIS) that can be used to obtain stigmatic EUV spectra within its 308–381 Å (NIS-1) and 513–633 Å (NIS-2) wavebands along its 240'' long slit. Several slit widths are available, the most commonly used being 4''. The instrument can be operated in a sit-and-stare mode wherein successive exposures over small (single slit) areas are obtained, or it can be used to obtain raster images of target areas by obtaining spectra from successive slit pointings. In the latter case, the CDS scans a region of the Sun from the West to East. Since the CDS pointing has no compensation for solar rotation during observations, the actual field-of-view (FOV) of an obtained spectroheliogram will be stretched out in the x-direction when the targeted region is located on the solar disk. In this study, the CDS rastering observation was made during 17:10:10–19:11:43 UT, consisting of 60 pointing positions. The FOV is 264'' × 237''. The pointing difference between CDS NIS-1 and NIS-2 has been corrected when applying *mk_cds_map* in the Solar Software (SSW) IDL library.

2.3. Coalignment

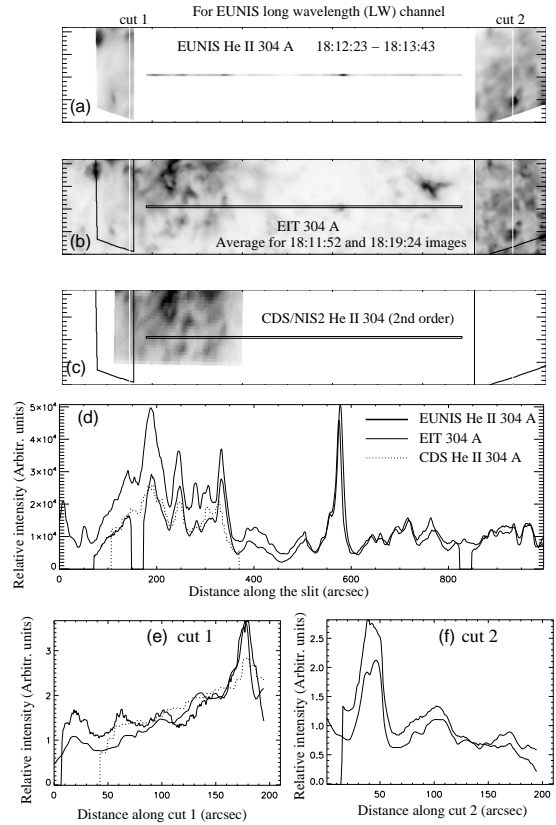


FIG. 3.— Comparisons of images and intensity profiles from observations of different instruments. (a) He II 304 Å line intensity image from the EUNIS-06 LW channel. The nearly-horizontal line in panels (a)-(c) represents the EUNIS LW slit. (b) The EIT 304 Å image, in which the contrast in the right lobe is enhanced in order to be seen clearly. (c) Image of the He II 304 Å (second order) line intensity from CDS/NIS-2. (d) Comparisons of intensity profiles along the EUNIS slit (including its extendings in two lobes). (e) and (f) Comparisons of intensity profiles along cut1 and cut2 (white vertical lines) marked in (a), respectively.

We used the EUNIS lobe images to precisely coalign EUNIS data with full disk solar images obtained with EIT. We first scaled the EIT images to the same pixel size as EUNIS. We then coaligned the left lobe of an EUNIS image with the EIT image by applying a cross-correlation technique. If the EUNIS image (or slit) is tilted to the East-West direction and its actual spatial scale is different from the design value, its right lobe will have offsets to the EIT image that has been coaligned by the left lobe. So we can estimate the tilt angle of the EUNIS slit and actual spatial resolution from the measurements of these offsets. For the EUNIS SW channel, we measured the offsets of $dx=4.7$ pixel in the x -direction and $dy=-20.6$ in the y -direction for the right lobe by comparing EUNIS Fe XI $\lambda 180$ image with the EIT $\lambda 195$ image. We then determined the actual pixel size from flight data by $R_{\text{flight}} \approx R_{\text{design}} D / (D + dx)$ where R_{flight} and R_{design} are the actual (from flight measurements) and designed (nominal) pixel sizes of EUNIS images, and D is the distance in EUNIS pixels between two lobe regions used for coalignments. The tilt angle of the EUNIS image (or slit) can be determined by $\theta \approx \tan^{-1}[dy / (D + dx)]$. From the solar measurements we obtained $R_{\text{flight}}=0''.922 \text{ pixel}^{-1}$ and $\theta=1.4^\circ$ counter-clockwise from the East-West. Similarly for the LW channel, we measured the offsets of the right lobe by

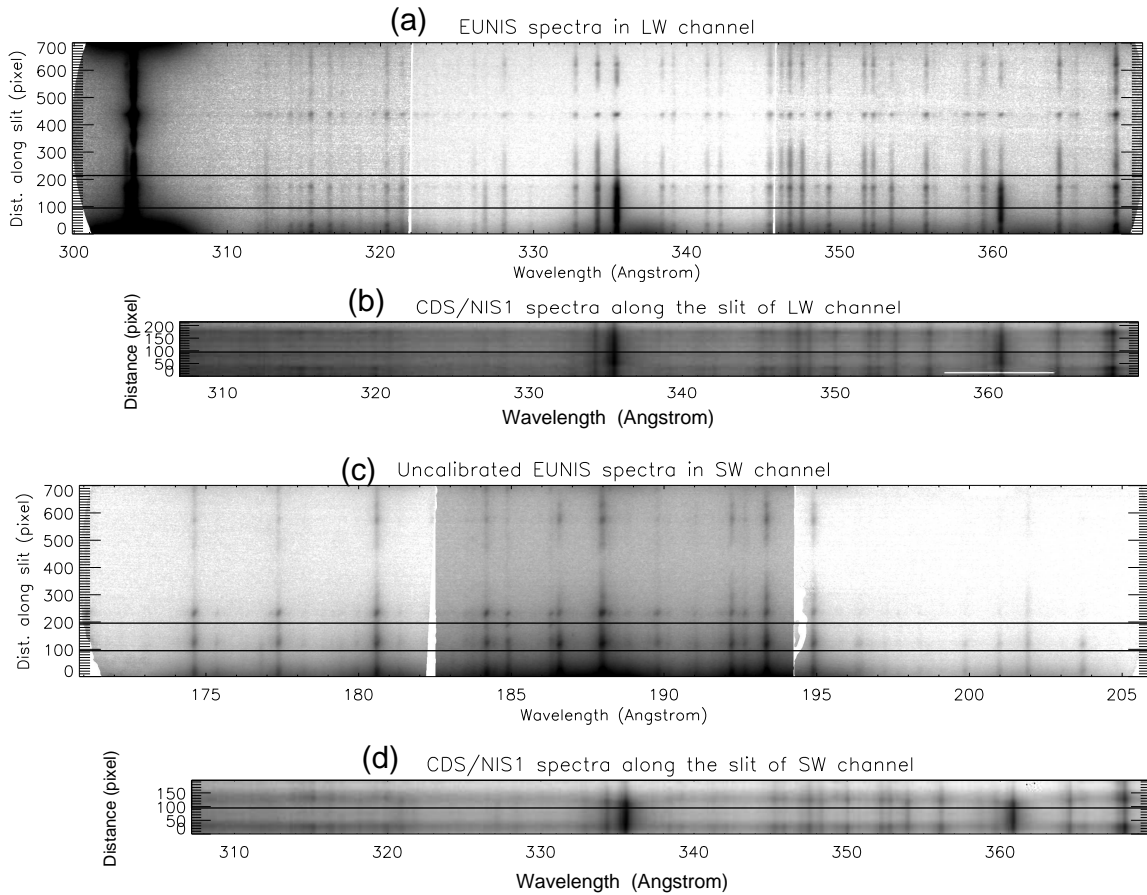


FIG. 4.— (a) EUNIS-06 full window spectra along the slit of LW channel, averaged for the data observed during 18:12:23 – 18:13:43 UT. (b) CDS/NIS-1 spectra extracted along the slit position of EUNIS LW. (c) EUNIS full window spectra along the slit of SW channel, averaged for the data observed during 18:12:23 – 18:13:43 UT. (d) CDS/NIS-1 full window spectra extracted along the slit position of EUNIS SW. In all panels, the spectra are shown as negative images, where darker areas correspond to greater intensities. The y-axis in all plots is in units of EUNIS pixels. In (a) and (b), two horizontal lines mark the same section (111'' wide) along the LW slit. In (c) and (d), two horizontal lines mark the same section (94'' wide) along the SW slit. The EUNIS and CDS spectra averaged in these sections are used to measure intensities of the lines used for radiometric calibration.

comparing EUNIS He II $\lambda 304$ image with the EIT $\lambda 304$ image, and obtained $R_{\text{flight}=0} = 0.927 \text{ pixel}^{-1}$ and $\theta = 1.0^\circ$. The measurements also show that the EUNIS-06 SW and LW slits were not co-pointing in flight, but were instead separated by about $76''$ in the y -direction (Fig. 1).

We coaligned the CDS images by comparing NIS-1 Mg IX $\lambda 368$, Si X $\lambda 347$, Fe XII/Fe XI $\lambda 352$ images with the EIT $\lambda 195$ image, and comparing NIS-2 He I $\lambda 584$ image with the EIT $\lambda 304$ image. The coalignment between CDS and EUNIS was made based on the average offsets measured above. Figure 1 shows positions of the FOVs for the coaligned EUNIS LW and SW channels, CDS NIS-1 and NIS-2, and TRACE relative to the EIT images. Figures 2 and 3 show the EUNIS SW and LW channel images and their comparisons with the coaligned EIT, TRACE and CDS/NIS images. A good agreement in their intensity profiles along two cuts in the lobe regions and along the EUNIS slit indicate that the images from the different instruments have been well coaligned.

3. RADIOMETRIC CALIBRATION OF EUNIS LW CHANNEL

Direct calibration of the EUNIS-06 LW channel was carried out in August 2006 at RAL in the same facility and using the same EUV light source as was used for pre-flight calibrations of CDS (Lang et al. 2002) and the EUV Imaging Spectrometer (EIS) (Culhane et al.

2007) on *Hinode*. Recalibration of the PTB light source against the primary EUV radiation standard of BESSY-II in March 2007 showed that it had remained stable within its 7% uncertainty. Measurements were made of the He II 304 Å line and of 11 distinct Ne features between 300 and 370 Å at 157 individual locations covering the instrument's entrance aperture. The aperture-averaged response at each wavelength was combined with the known source flux and with geometric factors, such as aperture area and pixel size, resulting in the absolute EUNIS response within a total uncertainty of 10% over its full LW bandpass (Thomas et al. 2008).

We validated the laboratory calibration of the EUNIS LW channel by checking its relative calibration using the density- and temperature-insensitive line ratio method (Brosius et al. 1998a,b). Table 1 lists six groups of emission lines for Mg VIII, Si VIII, Si IX, Fe XI, Fe XII, and Fe XVI. Column (3) gives the theoretical line intensity relative to the strongest one in each group, which were calculated with the CHIANTI (version 6) package (Dere et al. 1997, 2009). The line ratios exhibit slight variations with electron density (N_e), so we took the mean value over a range of $8.5 < \log_{10} N_e < 10.5$, and the uncertainty corresponds to half of the difference between the maximum and minimum values. In each case, the intensity ratios were calculated at the temperature

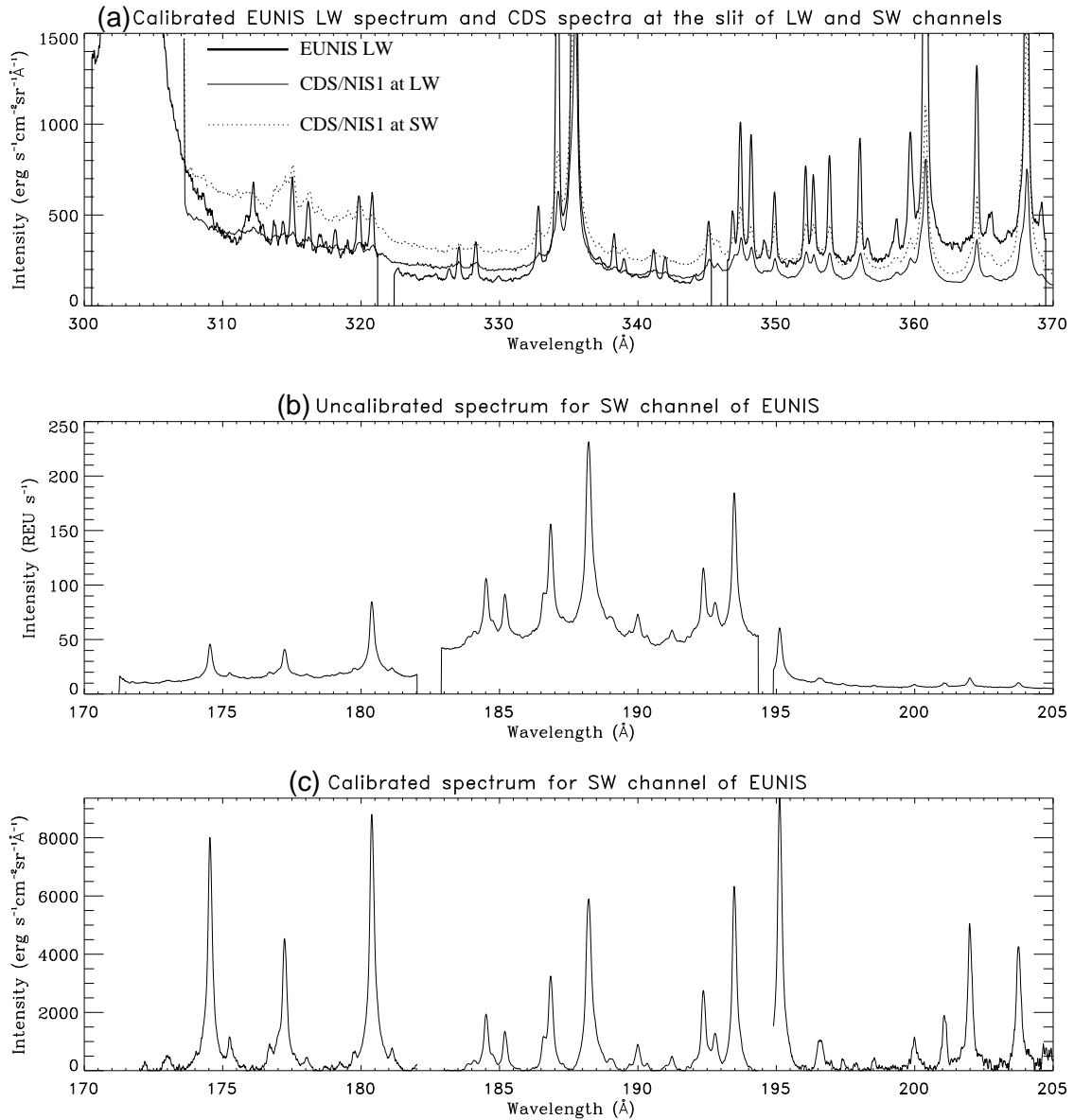


FIG. 5.— (a) Calibrated EUNIS/LW channel (thick solid line) and CDS/NIS-1 (thin solid line) spectra, spatially averaged over a segment along the LW slit shown in Fig. 4a and b. The CDS/NIS-1 spectrum, averaged over a segment along the SW slit shown in Fig. 4d, is also plotted (dotted line) for comparison. (b) The uncalibrated EUNIS/SW channel spectrum, spatially averaged over a segment shown in Fig. 4c. (c) Same as that shown in (b) but after background subtraction and application of the absolute radiometric calibration shown in Fig. 9b.

of maximum ion abundance (i.e., the lines' formation temperature), using the ionization equilibrium data (*chi-anti.ioneq*). Column (4) gives the observed intensities of calibrated spectral lines measured from the averaged spectra (see Fig. 4a and Fig. 5a), and column (5) the corresponding relative intensities to the same lines used in column (3) within each line group. Ideally, the values listed in column (5) should match those listed in column (3). Column (6) gives the ratio of the observed relative intensities to the theoretical ones, normalized by the weighted average ratio within each group. Ratios close to unity indicate good agreement between the observed and the theoretical values. Column (6) in Table 1 reveals that all but three of the ratios agree to within one standard deviation (1σ) of measurements and that all of them agree within factors better than 2. This is illustrated in Figure 6, where the values in column (6) are plotted as

a function of wavelength. The fact that many line intensity ratios from different elements and ionization stages yield mutually consistent results supports both the general validity of the atomic physics calculations and our laboratory calibration of the EUNIS LW channel at RAL.

4. CDS UNDERFLIGHT CALIBRATION WITH EUNIS LW

The lab-calibrated SERTS-97 was successfully used to improve the sensitivity curve for the CDS NIS-1 waveband based on their coordinated, cospatial spectra (Thomas 2002). In the following, we present a new calibration update for CDS NIS-1 based on the EUNIS LW observation, and then apply this updated CDS response to calibrate the EUNIS SW channel in the next section.

Figures 4a and 4b show the time-averaged EUNIS LW spectra and the cospatial CDS NIS-1 spectra. CDS NIS-1 and EUNIS made coordinated observations of AR 10871,

TABLE 1
EUNIS-06 LW CHANNEL CALIBRATION VERIFICATION FROM DENSITY- AND
TEMPERATURE-INSENSITIVE LINE RATIOS.

Ion	Wavelength (Å)	Theo. Rel. Intensity (3)	Observed Intensity (ergs cm ⁻² s ⁻¹ sr ⁻¹) (4)	Observed Rel. Intensity (5)	Normalized Col.(5)/Col.(3) (6)
(1)	(2)	(3)	(4)	(5)	(6)
Mg VIII.....	313.75	0.357± 0.021	28.53± 2.85	0.252± 0.036	0.823± 0.126
	315.04	1.000± 0.000	113.09± 11.31	1.000± 0.100	1.165± 0.116
	317.04	0.252± 0.015	25.17± 2.67	0.223± 0.032	1.029± 0.162
	339.01	0.229± 0.005	18.40± 6.03	0.163± 0.056	0.828± 0.284
Si VIII.....	314.33	0.336± 0.000	30.84± 3.08	0.333± 0.047	0.946± 0.134
	316.21	0.670± 0.000	80.97± 8.10	0.873± 0.123	1.245± 0.176
	319.83	1.000± 0.000	92.73± 9.27	1.000± 0.100	0.955± 0.096
Si IX.....	341.99	0.362± 0.030	33.66± 6.37	0.347± 0.074	0.964± 0.221
	345.12 ^a	1.000± 0.000	97.13± 9.71	1.000± 0.100	1.007± 0.101
Fe XI.....	341.11	0.281± 0.039	44.57± 6.55	0.334± 0.059	1.161± 0.262
	352.66	1.000± 0.000	133.61± 13.36	1.000± 0.100	0.978± 0.098
Fe XII.....	346.85	0.304± 0.002	75.19± 8.68	0.276± 0.042	0.969± 0.148
	352.11	0.604± 0.011	142.45± 14.25	0.523± 0.074	0.924± 0.132
	364.47	1.000± 0.000	272.14± 27.21	1.000± 0.100	1.066± 0.107
Fe XVI.....	360.761	0.480± 0.000	1299.37± 129.94	0.512± 0.072	1.046± 0.148
	335.410	1.000± 0.000	2536.80± 253.68	1.000± 0.100	0.980± 0.098

^a Si IX 345.12 was self-blended with 344.95.

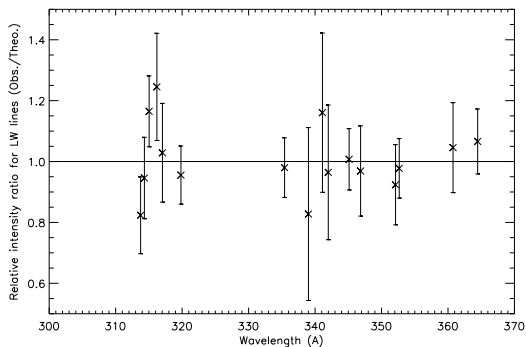


FIG. 6.— Plot of the observed-to-theoretical intensity ratios (col.[6] of Table 1), normalized to the weighted average ratio within each line group, as a function of wavelength for the EUNIS LW channel.

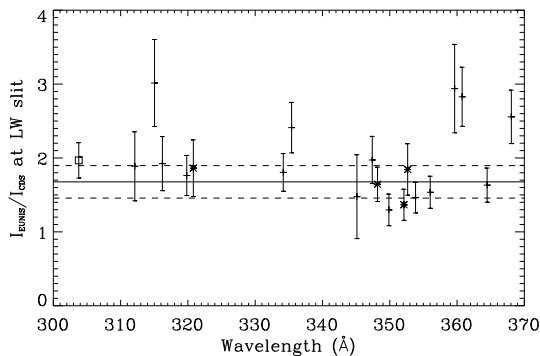


FIG. 7.— Plot of the EUNIS/LW-to-CDS/NIS-1 intensity ratios for the spectral lines listed in Table 2. The solid line represents the average ratio for those lines with the ratios less than 2 and the dashed lines their standard deviation. Intensity ratios in excess of 2 are discussed in the text. The data points denoted with *asterisks* indicate members of temperature- and density-insensitive line groups used for calibration of the EUNIS SW channel. The point denoted with a *box* corresponds to the He II 303.78 Å line of CDS NIS-2 in second order.

which was located near the eastern end of the EUNIS slit. To reduce the effect of scattered light from the EUNIS lobe, we averaged the spectra along the slit over an area away from that lobe. Figure 5a shows a comparison between the averaged spectra in the wavelength range from 300 to 380 Å, which clearly indicates that EUNIS has much higher sensitivity and spectral resolution than CDS. Especially for spectral lines of CDS in the wavelength range 310–330 Å, the measurement of line intensities is challenging because the lines are weak and not well separated. We fitted the EUNIS spectral lines with Gaussian functions and fitted the CDS lines with broadened Gaussian functions (Thompson 1999) using the standard SSW line profile fitting routine (*xcfit.pro*). Thompson (1999) found that the broadened Gaussian function appears to well match the line profiles of the post-recovery CDS data after the attitude-loss of SOHO in 1998.

Table 2 lists 20 emission lines observed in both EUNIS LW and CDS (NIS-1 in first order and NIS-2 in second order) and their measured intensities with a 1σ uncertainty. For CDS, absolute intensities are based on the previously most recent rocket underflight calibrations implemented on 28 Feb 2000 based on EGS (the EUV Grating Spectrometer; Woods et al. 1998) and SERTS-97 (Lang et al. 2002; Thomas 2002). (Out of these lines, four were selected to calibrate the EUNIS SW bandpass based on their membership in insensitive line groups that include lines scattered throughout the SW bandpass, as described below.) The He II $\lambda 304$ line is a second order line of NIS-2. Since in the EUNIS LW bandpass the scattered light from the lobe image around this line is very strong (Fig. 4a), we chose a smaller area from pixel No. 142 to 214 along the slit to reduce this effect as much as possible. Note that Si XI $\lambda 303$ is another NIS-2 second-order line, but as it is too weak to be reliably separated from the strong He II line in the CDS spectrum, we did

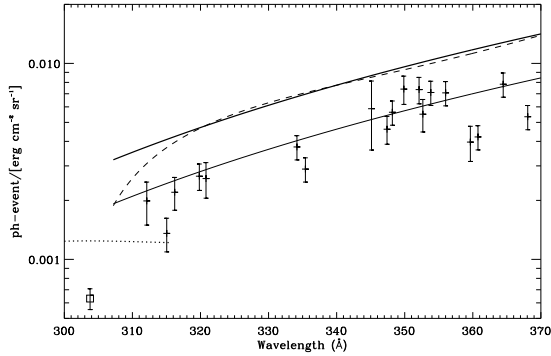


FIG. 8.— The ratio of CDS intensities in detector photon-event units to those measured by EUNIS-06 in absolute units. The thin solid line represents the updated CDS calibration by EUNIS, obtained by reducing the present SSW calibration curve for CDS NIS-1 (thick solid line) by a factor of 1.68 (the average EUNIS-to-CDS line ratio). The dotted line represents the present SSW calibration curve for the CDS NIS-2 second order spectra. The dashed line represents the SERTS-97 underflight recalibration curve for the CDS NIS-1 (Thomas 2002).

not include its measurements here. The EUNIS LW to CDS line intensity ratios are given in column 5 of Table 2 and shown in Figure 7. We suspect that the CDS sensitivity in the spectral vicinities of the strongest lines in our spectra (Fe XVI at 335.4 and 360.8 Å, Mg IX at 368.1, and Mg VIII at 315.0 Å) are reduced even more than the typical value $\lesssim 2$ due to detector burn-in by persistent exposure to these strong lines. For this reason we averaged over only those lines with the EUNIS-to-CDS line ratios less than 2 to obtain their relative calibration factor, which is 1.68 ± 0.22 . This factor is a correction to the previous CDS calibration, which indicates that the response efficiency of CDS NIS-1 has decreased by a factor of about 1.7 in the nine years between absolute calibration updates. The measurements also indicate that the response efficiency of CDS NIS-2 in the second order at 303–304 Å has decreased by a factor of about 2 during this time interval. These results are in very good agreement with a recent radiometric calibration correction for CDS NIS by Del Zanna et al. (2010) who also found a factor of about 2 decrease in responsivity for most wavelengths over 10 years.

Figure 8 shows comparisons between the EUNIS-06 underflight recalibration curve and the presently used calibration curves for CDS NIS in SSW. Here the EUNIS-06 recalibration curve was obtained by reducing the present SSW calibration curve for CDS NIS-1 by a factor of 1.68 (the average EUNIS-to-CDS line intensity ratio). The units are photon-events/($\text{erg cm}^{-2}\text{sr}^{-1}$), where the term “photon-events” refers to the photons which have actually been detected by the instrument, as opposed to photons which impinge on the detector.

5. ABSOLUTE CALIBRATION OF EUNIS SW BANDPASS

We used the newly calibrated CDS NIS-1 bandpass to calibrate the EUNIS SW channel by means of density- and temperature-insensitive line intensity ratios because the efficiency of the EUNIS-06 SW bandpass could not be directly measured at RAL. The insensitive line ratio method was proposed by Neupert & Kastner (1983) as a means of monitoring relative calibration variations of inflight EUV spectrometers and was used by Thomas & Neupert (1994) and Brosius et al. (1996) to

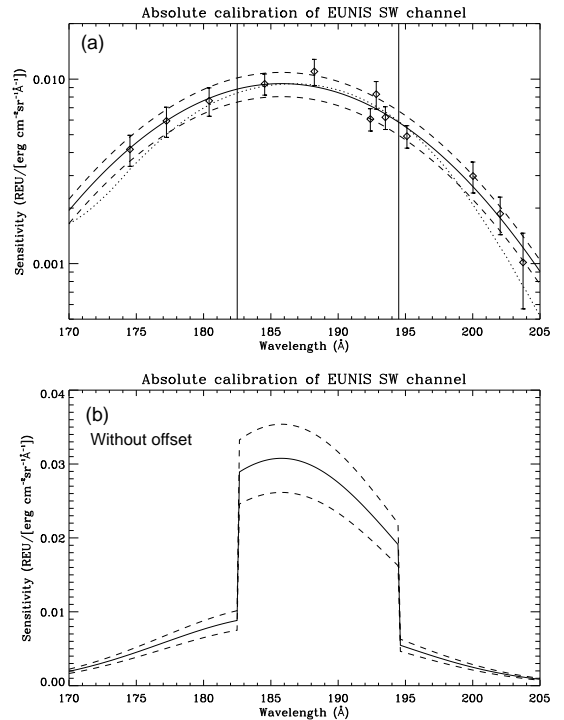


FIG. 9.— (a) The measured instrument sensitivity using density- and temperature-insensitive line intensity ratios. The thick solid curve is a least-square parabolic fit to the data points. The dashed lines indicate the 15% uncertainty. The dotted line represents the relative calibration curve derived by combining measurements of individual optical components, which has been scaled to best match the data points. (b) The same calibration curves as in (a) but on a linear scale and without correction of relative sensitivity factors for the detectors ($f_{\text{sensitivity}}$ in Eq. (1)).

adjust the laboratory calibration curve for SERTS-89, SERTS-91 and SERTS-93. Brosius et al. (1998a,b) derived the SERTS-95 relative radiometric calibration for both the first-order and second-order wave bands with this technique.

The CDS measurements were used because the EUNIS LW and SW channels were not precisely co-pointed in observation. Figures 4c and 4d show the cospatial spectra of EUNIS SW and CDS NIS-1 bandpasses along their slits. Figures 5a and 5b show the spectra averaged over just the same spatial area for both instruments. We measured the intensities of spectral lines for both the EUNIS SW data and the CDS NIS-1 data with a broadened Gaussian fit. The measured CDS line intensities were then corrected for calibration update by multiplying a factor of 1.68 (the average EUNIS-to-CDS line intensity ratio).

We used the CHIANTI package to obtain theoretical values for density- and temperature-insensitive line intensity ratios between 5 emission lines observed by CDS NIS-1 and 12 lines observed by EUNIS SW. These include lines from Fe X to Fe XIII listed in Table 3. The first two columns of Table 3 provide ion name and line pairs, and the third column provides the theoretical line intensity ratios. By assuming that the observed line intensity ratio is equal to the theoretical one for each line pair, we obtained the sensitivity (or efficiency) of EUNIS SW channel at wavelengths for those selected lines. Note that the fiber-optic coupling between the MCP and the APS arrays in each optical channel leads to differences

TABLE 2
ABSOLUTELY CALIBRATED ACTIVE REGION LINE LISTS FOR EUNIS LW AND CDS
NIS-1/NIS-2 BANDPASSES

Wavelength ^a (Å)	Ion	EUNIS Intensity (ergs cm ⁻² s ⁻¹ sr ⁻¹)	CDS Intensity (ergs cm ⁻² s ⁻¹ sr ⁻¹)	EUNIS-to-CDS Intensity Ratio
303.78 ^o	He II	14272.1±1427.2	7253.1± 502.3	1.97±0.24
312.11	Fe XIII	90.5 ±9.1	48.0±10.9	1.89±0.47
315.04	Mg VIII	113.1±11.3	37.5±6.3	3.01±0.59
316.21	Si VIII	81.0±8.1	42.1±6.8	1.92±0.37
319.83	Si VIII	92.7±9.3	52.6±6.2	1.76±0.27
320.81*.....	Fe XIII	98.1±9.8	52.7±9.5	1.86±0.38
334.17	Fe XIV	586.7±58.7	325.1±32.5	1.80±0.26
335.41	Fe XVI ^b	2714.2±271.4	1125.9±112.6	2.41±0.34
345.12	Si IX ^c	97.1±9.7	65.8±24.4	1.48±0.57
347.40	Si X	222.7±22.3	112.9±14.4	1.97±0.32
348.18*.....	Fe XIII	194.1±19.4	118.1±11.8	1.64±0.23
349.87	Si IX	103.2±10.3	79.6±10.4	1.30±0.21
352.11*.....	Fe XII	142.5±14.3	104.3±12.2	1.37±0.21
352.66*.....	Fe XI	133.6±13.4	72.4±11.6	1.84±0.35
353.83	Fe XIV	150.8±15.1	103.0±10.3	1.46±0.21
356.01	Si X	184.5±18.5	120.2±12.0	1.54±0.2
359.64.....	Fe XIII ^d	168.3±16.8	57.3±10.1	2.94±0.60
360.76	Fe XVI	1299.4±130.0	459.5±46.0	2.83±0.40
364.47.....	Fe XII	272.1±27.2	166.7±16.7	1.63±0.23
368.07	Mg IX ^e	902.8±90.3	353.1±35.3	2.56±0.36

^a The line wavelength data are taken from CHIANTI line list. Those lines marked with *asterisks* are members of temperature- and density-insensitive line groups which were used to calibrate the EUNIS SW bandpass. The line marked with a *diamond* is a second order line in CDS NIS-2.

^b Fe XVI 335.41 was blended with Mg VIII 335.25.

^c Si IX 345.12 was self-blended with 344.95.

^d Fe XIII 359.64 was self-blended with 359.84.

^e Mg IX 368.07 was blended with Mg VII 367.67 and 367.68.

TABLE 3
DENSITY- AND TEMPERATURE-INSENSITIVE LINE GROUPS SELECTED FOR EUNIS SW
CALIBRATION. THE RELATIVE LINE INTENSITY USED IN CALCULATION OF THEORETICAL LINE
RATIOS IS IN UNITS OF ERG.

Ion (1)	Line Pairs (2)	Theoretical ^a (3)	Measured ^b (4)	Col.(4)/Col.(3) (5)	Sensitivity ^c (6)
Fe X.....	345.72/174.53	0.048±0.007	0.049±0.008	1.020±0.220	4.164±0.797
	345.72/177.24	0.087±0.012	0.089±0.014	1.020±0.214	5.939±1.105
	345.72/184.54	0.201±0.008	0.200±0.039	0.994±0.196	9.428±1.239
Fe XI.....	352.66/180.41	0.082±0.006	0.084±0.016	1.030±0.208	7.628±1.338
	352.66/188.23	0.127±0.004	0.105±0.020	0.824±0.157	11.009±1.789
	352.66/192.83 ^d	0.771±0.033	0.654±0.123	0.849±0.164	8.288±1.417
Fe XII.....	352.11/192.39	0.311±0.014	0.368±0.060	1.184±0.201	6.075±0.841
	352.11/193.51	0.148±0.008	0.154±0.025	1.040±0.179	6.210±0.876
	352.11/195.12	0.094±0.002	0.102±0.017	1.090±0.180	4.905±0.683
Fe XIII....	320.81/200.02	0.541±0.013	0.581±0.112	1.074±0.209	2.984±0.570
	320.81/203.74	0.112±0.009	0.138±0.026	1.230±0.252	1.015±0.447
	348.18/202.04	0.148±0.021	0.148±0.026	0.999±0.227	1.864±0.430

^a Theoretical line intensity ratios calculated with the CHIANTI package (ver.6).

^b The measured CDS to EUNIS SW line intensity ratios, where the EUNIS SW is after calibration shown in Fig. 9b.

^c The sensitivity is in units of 10⁻³ REU/[erg cm⁻²sr⁻¹Å⁻¹] for the SW lines.

^d Fe XI λ 192.83 is blended with a flare line, Ca XVII λ 192.82 (an EIS “core line” formed at T=5×10⁶ K), whose contribution is expected to be small in the present case.

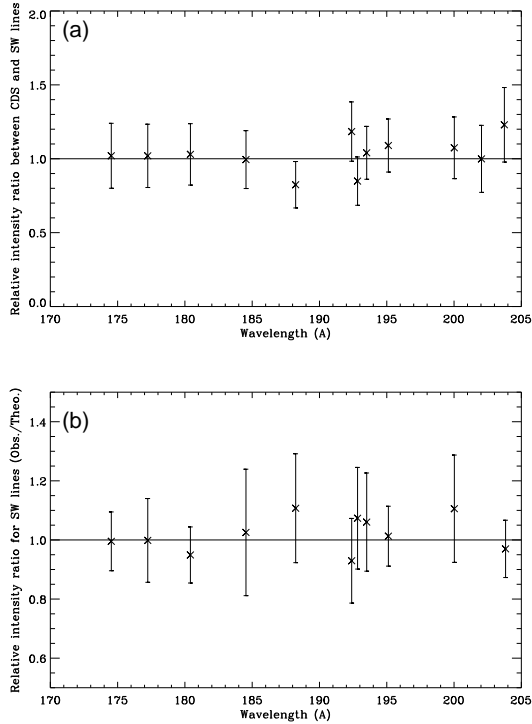


FIG. 10.— (a) Plot of the observed-to-theoretical intensity ratios between CDS and SW lines (col.[5] of Table 3) as a function of wavelength. (b) Plot of the observed-to-theoretical intensity ratios (col.[6] of Table 4), normalized to the weighted average ratio within each line group, as a function of wavelength for the EUNIS SW channel.

in the overall sensitivity of each APS array relative to the other two. However, these differences are uniform over any given APS and are easily measured during flat-field testing. After correcting for these factors (g_i), the response of the three APS arrays should be a smoothly varying curve as a function of wavelength. Figure 9a shows the obtained sensitivities after this correction [Column (6) of Table 3] and a least-square parabolic fitting on a logarithmic scale. The absolute calibration response curve ($f_{\text{sensitivity}}$) in the range of 170–205 Å was obtained by,

$$f_{\text{sensitivity}} = g_i 10^{R(\lambda)}, \quad (1)$$

$$R(\lambda) = a_0 + a_1(\lambda - \lambda_0) + a_2(\lambda - \lambda_0)^2, \quad (2)$$

where $R(\lambda)$ is the fitting function with $\lambda_0=187.5$ Å, $a_0=-2.03\pm 0.03$, $a_1=-(9.5\pm 2.8)\times 10^{-3}$, $a_2=-(2.8\pm 0.3)\times 10^{-3}$, and g_i are the relative sensitivity factors for the three APS arrays, given by

$$g_i = \begin{cases} 1.000 & (170 < \lambda < 182.5 \text{ \AA}) \\ 3.254 & (182.5 < \lambda < 194.5 \text{ \AA}) \\ 0.950 & (194.5 < \lambda < 205 \text{ \AA}) \end{cases}. \quad (3)$$

The shape of the response curve derived from solar observations matches well with that of a relative calibration curve derived by combining measurements of individual optical components (Fig. 9a).

We absolutely calibrated the average spectrum of the EUNIS-06 SW channel using the response function derived above. Figure 5c shows the calibrated SW spectrum, where the background emission has been removed. To further demonstrate the validity of SW calibration

derived above, we measured absolute intensities of the 12 iron lines selected for the calibration from the calibrated spectra by refitting these lines. The resultant observed line intensity ratios for density- and temperature-insensitive line pairs from CDS NIS-1 and EUNIS SW are listed in column (4) of Table 3. A line-by-line comparison demonstrates good agreement between theoretical and observed values. This is illustrated in Figure 10a, where we plot the ratios and associated uncertainties of the observed-to-theoretical intensity ratios (col. [5] of Table 3) as a function of wavelength. The standard deviation of these ratios relative to 1 is about 15%. The fact that no slope is evident in this figure indicates that there is no wavelength bias in the derived absolute radiometric calibration curve.

In addition, we examined the relative radiometric calibration of the EUNIS SW channel using the same method used for the LW channel. Table 4 lists four groups of emission lines from Fe X to Fe XIII, in which column (3) gives the theoretical line intensity relative to the strongest one in each group. Column (4) gives the observed intensities of calibrated spectral lines measured from the averaged spectrum (Fig. 5c), and column (5) the corresponding relative intensities. Column (6) gives the ratio of the observed relative intensities to the theoretical ones, further normalized by the weighted average ratio within each group. These are plotted in Figure 10b. All of the ratios are equal to unity within their 1σ measurement uncertainties, and their maximum deviation is less than 15%.

Therefore, the results from Figures 10a and 10b suggest that the uncertainty (σ_1) in the relative calibration of the EUNIS SW channel is about 15%. Other errors that affect our result include the 10% uncertainty (σ_2) in the absolute calibration of the EUNIS-06 LW channel (see Sect. 3) and the typical uncertainty (σ_3) of about 10% in the theoretically predicted line intensity ratios used in this procedure (estimated from those listed in column (3) of Table 3). Thus, we estimate that the absolute radiometric calibration of the EUNIS-06 SW channel derived here is accurate to $\pm 20\%$ overall (using $\sqrt{\sigma_1^2 + \sigma_2^2 + \sigma_3^2}$).

6. SUMMARY

Using coordinated, cospatial spectroscopic observations of an active region, the lab-calibrated EUNIS LW channel has been applied to update the CDS NIS calibration. The improved CDS NIS sensitivity curve was then used to derive the EUNIS-06 SW absolute radiometric calibration by applying a technique based on density- and temperature-insensitive line intensity ratios. Many such ratios of iron lines are mutually consistent and yield an instrumental response curve that matches well to that derived by combining measurements of individual optical components. This result supports the accuracy of the atomic physics parameters. Since the EUNIS SW channel has a wavelength range covering wavebands of TRACE and SOHO/EIT, the absolutely calibrated SW spectra can be used to provide underflight calibration updates for these instruments. In addition, data from the second successful EUNIS flight (EUNIS-07, launched on 2007 November 6), will be used to provide a calibration update for Hinode/EIS using similar techniques.

The EUNIS program is supported by the NASA Helio-

TABLE 4
EUNIS-06 SW CHANNEL CALIBRATION VERIFICATION FROM IRON LINE RATIOS.

Ion (1)	Wavelength (Å) (2)	Theo. Rel. Intensity (3)	Observed Intensity (ergs cm ⁻² s ⁻¹ sr ⁻¹) (4)	Observed Rel. Intensity (5)	Normalized Col.(5)/Col.(3) (6)
Fe X	174.531	1.000± 0.000	2556.87± 255.69	1.000± 0.100	0.995± 0.100
	177.240	0.550± 0.007	1411.20± 141.12	0.552± 0.078	0.998± 0.142
	184.537	0.238± 0.025	626.42± 93.03	0.245± 0.044	1.025± 0.214
Fe XI	180.408	1.000± 0.000	3061.00± 306.10	1.000± 0.100	0.949± 0.095
	188.232	0.692± 0.061	2469.34± 246.93	0.807± 0.114	1.107± 0.184
	192.830	0.114± 0.009	394.99± 39.50	0.129± 0.018	1.073± 0.172
Fe XII	192.394	0.303± 0.019	847.44± 84.74	0.278± 0.039	0.930± 0.143
	193.509	0.634± 0.043	2027.08± 202.71	0.664± 0.094	1.060± 0.166
	195.119	1.000± 0.000	3052.26± 305.23	1.000± 0.100	1.013± 0.101
Fe XIII ...	200.022	0.208± 0.015	281.62± 30.45	0.237± 0.035	1.106± 0.182
	203.828	1.000± 0.000	1188.14± 118.81	1.000± 0.100	0.970± 0.097

physics Division through its Low Cost Access to Space Program in Solar and Heliospheric Physics. The authors thank the entire EUNIS team for the concerted effort that led to a successful first flight. TJW is grateful to Dr. William T. Thompson for his valuable comments on CDS calibration. The work of TJW was supported by NRL grant N00173-06-1-G033. The authors also thank the anonymous referee for valuable suggestions. Radiometric calibration of the EUNIS-06 instrument was made possible by financial contributions and technical support from both the Rutherford-Appleton Laboratory in England and the Physikalisch-Technische Bundesanstalt in Germany, for which we are very grateful. CHIANTI is a collaborative project involving the NRL (USA), the Universities of Florence (Italy) and Cambridge (UK), and George Mason University (USA).

REFERENCES

- Andretta, V., Jordan, S. D., Brosius, J. W., Davila, J. M., Thomas, R. J., Behring, W. E., Thompson, W. T., & Garcia, A. 2000, *ApJ*, 535, 438
- Brosius, J. W., Davila, J. M., & Thomas, R. J. 1998a, *ApJ*, 497, L113
- Brosius, J. W., Davila, J. M., & Thomas, R. J. 1998b, *ApJS*, 119, 255
- Brosius, J. W., Davila, J. M., Thomas, R. J., & Monsignori-Fossi, B. C. 1996, *ApJS*, 106, 143
- Brosius, J. W., Davila, J. M., Thomas, R. J., Saba, J. L. R., Hara, H., & Monsignori-Fossi, B. C. 1997, *ApJ*, 477, 969
- Brosius, J. W., Rabin, D. M., & Thomas, R. J. 2007, *ApJ*, 656, L41
- Brosius, J. W., Rabin, D. M., & Thomas, R. J. 2008, *ApJ*, 682, 630
- Brosius, J. W., Rabin, D. M., Thomas, R. J., & Landi, E. 2008, *ApJ*, 677, 781
- Brosius, J. W., Thomas, R. J., & Davila, J. M. 1999, *ApJ*, 526, 494
- Brosius, J. W., Thomas, R. J., Davila, J. M., & Landi, E. 2000, *ApJ*, 543, 1016
- Culhane, J. L., et al. 2007, *Sol. Phys.*, 186, 207
- Delaboudinière, J.-P., et al. 1995, *Sol. Phys.*, 162, 291
- Del Zanna, G., Andretta, V., Chamberlin, P. C., Woods, T. N., & Thompson, W. T. 2010, *A&A*, submitted
- Dere, K. P., Landi, E., Mason, H. E., Monsignori Fossi, B. C., & Young, P. R. 1997, *A&AS*, 125, 149
- Dere, K. P., Landi, E., Young, P. R., Del Zanna, G., Landini, M., & Mason, H. E. 2009, *A&A*, 498, 915
- Handy, B. N., et al. 1999, *Sol. Phys.*, 187, 229
- Harrison, R. A., et al. 1995, *Sol. Phys.*, 162, 233
- Jess, D. B., Rabin, D. M., Thomas, R. J., Brosius, J. W., Mathioudakis, M., & Keenan, F. P. 2008, *ApJ*, 682, 1363
- Lang, J., Thompson, W. T., Pike, C. D., et al., in *The Radiometric Calibration of SOHO*, eds. A. Pauluhn, M.C.E. Huber and R. von Steiger, ESA SR-002, p.105
- Neupert, W. M. & Kastner, S. O. 1983, *A&A*, 128, 188
- Neupert, W. M., Epstein, G. L., Thomas, R. J., & Thompson, W. T. 1992, *Sol. Phys.*, 137, 87
- Rabin, D. M., Thomas, R. J., & Brosius, J. W. 2008, in *AGU Spring Meeting*, abstract SP51A-07
- Thomas, R. J. 2002, in *The Radiometric Calibration of SOHO*, eds. A. Pauluhn, M.C.E. Huber and R. von Steiger, ESA SR-002, 225
- Thomas, R. J., & Davila, J. M. 2001, *Proc. SPIE*, 4498, 161
- Thomas, R. J., & Neupert, W. M. 1994, *ApJS*, 91, 461
- Thomas, R. J., Wang, T. J., Rabin, D. M., Jess, D. B., & Brosius, J. W., 2008, in the Meeting of Joint Assembly AGU/SPD meeting
- Thompson, W. 1999, *CDS Software note No.53* (<http://solar.bnsc.rl.ac.uk/software/notes.shtml>)
- Woods, T. N., Rottman, G. J., Bailey, S. M., Solomon, S. C., & Worden, J. R. 1998, *Sol. Phys.*, 177, 133